Computation of Spherical Harmonics Based Sound Source Directivity Models from Sparse Measurement Data

COMPUTATION OF SPHERICAL HARMONICS BASED SOUND SOURCE DIRECTIVITY MODELS FROM SPARSE MEASUREMENT DATA

Jens Ahrens
Chalmers University of Technology
412 96 Gothenburg, Sweden
jens.ahrens@chalmers.se

Stefan Bilbao
Acoustics and Audio Group/Reid School of Music
University of Edinburgh, Edinburgh, United Kingdom
s.bilbao@ed.ac.uk

ABSTRACT

Models of sound source directivity that are based on spherical harmonics have been applied in diverse scenarios including wave-based room acoustic simulation, spatial audio, and urban sound propagation. The measurement of directivities of real-world sound sources that are not electroacoustic transducers exhibits fundamental limitations in terms of the accuracy and spatial resolution than can be achieved. Particularly if the directivity is measured only in a plane or over a limited solid angle range, a classical spherical harmonic representation cannot be computed. In many cases it is also such that angle-dependent directivity data are available only at a sparse set of frequencies. We demonstrate in this paper that complete spherical-harmonics-based directivity models can be obtained from such sparse measurement data by interpolating the available data over both the angle and the frequency and then imposing the result onto a spherical wave. We present results based on publicly available directivity data for the human voice as well as for directivity data in the Common Loudspeaker Format. The presented directivity models are available for download.

1. INTRODUCTION

Representations of sound source directivity in terms of spherical harmonic (SH) expansion coefficients have been demonstrated to be an excellent match to advanced applications like wave-based room acoustic simulation [1] and virtual reality applications [2]. While geometrical acoustic simulations often use directivity data subsumed in frequency bands, the SH-based representations require a complete model of the directivity, particularly w.r.t. to time/frequency.

Directivity is usually measured with a microphone array that encloses the sound source (or a corresponding sequence of single-point measurements). A significant number of datasets of the directivities of various types of sound sources have been acquired, and some are publicly available. These include the human voice when talking and singing (see, for example, [3] and the references therein), musical instruments (see, for example, [4] and the references therein), as well as loudspeakers (for example, on the website accompanying the Common Loudspeaker Format CLF [5] or in [6, 7]). Data on machinery tend to be more limited but are available for vehicles such as cars [8], trains [9], and wind turbines [10], for example.

There are no fundamental limitations in the measurement of loudspeaker directivities as arbitrary measurement signals can be employed. Still, most available databases provide data only at selected frequencies or averaged over frequency bands. The situation is fundamentally different when considering musical instruments, machinery, or other radiating objects that are not electroacoustic transducers. In these cases, there are fundamental limitations in terms of how the source can be excited, as the source itself is difficult or impossible to separate from the instrument/machine behaviour. In [4], for example, the directivities of musical instruments were measured by having trained musicians play steady notes, identifying the stable partial oscillations, and manually reading magnitudes and phases at the corresponding frequencies from the signals captured by the microphones of the surrounding array. Machinery will require measuring quantities like the time-averaged sound pressure radiated in different directions.

What most—if not all—directivity data for non-electrocoustical sound sources have in common is that frequency-domain data is sparsely sampled. This requires interpolation in frequency, which is straightforward for magnitude spectra but not possible for phase spectra as we will explain in Sec. 2. It is not possible to compute complete SH models of directivities without phase information because the phase information encodes a significant amount of information on the curvature of the radiated wave. This technically excludes all data mentioned above. Note that the reconstruction of time signals from the magnitude spectrum as in [11] constitutes a different scenario as no interchannel dependency via the wave equation is apparent.

In this paper, we illustrate how the approach presented in [2, 12] can be used to augment such sparse directivity data to obtain a complete SH-based model. The approach essentially consists of imposing a wave front curvature on the directivity. This allows for the required interpolation to be performed. We present two examples: 1) A loudspeaker directivity that is available at densely sampled direction but only at a sparse set of frequencies and only in terms of the magnitude. This example is inspired by CLF. 2) The directivity of a singing voice that is available densely with respect to frequency but sparse with respect to the direction.

2. THE LIMITATIONS OF PHASE INTERPOLATION

In this section, we demonstrate the fundamental limitations that arise when interpolating a phase spectrum. The principles apply to both interpolation along the frequency as well as along the angle. Interpolation along the frequency has shown to be very problematic with undersampled spectra whereas interpolation along the angle seems less critical. Some insight into phase interpolation along the angle is available [13, 14] but final conclusions cannot be drawn. Note that computing a spherical harmonic representation of a directivity in frequency domain based on measurements at discrete angles constitutes an interpolation along the angle. Contradictory results have been presented, for example, on whether separate interpolation of magnitude and phase of head-related transfer functions or binaural room transfer functions along the angle is favorable over interpolation of the complex spectrum [14–16].

Assume that the sampling of the frequency axis in the data under consideration fulfils the Nyquist criterion. In this case, unwrapping has to be applied before any considerations of interpolation along the frequency can be made. As an example, assume that the measured directivity of a sound source that produces a perfect spherical wave is available on a given grid of measurement locations. A high signal-to-noise ratio (SNR) of the resulting transfer functions requires the sound source to produce a sufficient sound pressure level across the entire frequency range. All compact real-world sound sources are inefficient radiators at low frequencies so that a noisy transfer function has to be expected at the corresponding frequency bins. The DC bin is purely real so that its phase is always guaranteed to be 0 [17]. Assume that solely the frequency bin with index $k = 1$ is noisy so that the measured transfer functions are all identical at all bins with index $k > 1$. The phase of the transfer function at bin 1 might be -0.9π at a given measurement location and, say, $0.9\ \pi$ in an adjacent measurement location (cf. Fig. 1(a)). After unwrapping, this results in a phase offset of 2π between the two measurement locations for all bins at $k > 1$ as depicted in Fig. 1(a). Note that the information is still identical at the said bins, it is only the representation of the information that deviates.

Interpolating between the two given measurement locations will result in a phase spectrum that is offset by π at the direction half-way between the two measurement locations. A phase offset of π is equivalent to a change of the algebraic sign of the signal as

$$|S(\omega)| \cdot \mathrm{e}^{\mathrm{i}\angle S(\omega) \pm \pi} = -\,|S(\omega)| \cdot \mathrm{e}^{\mathrm{i}\angle S(\omega)} = -S(\omega)\,. \quad (1)$$

In other words, interpolation of the spherical wave between two measurement locations may produce a lobe flanked by two nulls. Recall that one single noisy bin is sufficient for this to occur.

Similar limitations arise with data that are not available at all frequencies. Unwrapping of the phase is not possible with such data, which can result is similar issues as described above. Fig. 1(b) illustrates this. It is indeed possible to impose a linear phase slope onto the sparse data to model the propagation delay that the directivity comprises. One may unwrap based on this. However, the same issues that were illustrated in Fig. 1(a) are still apparent.

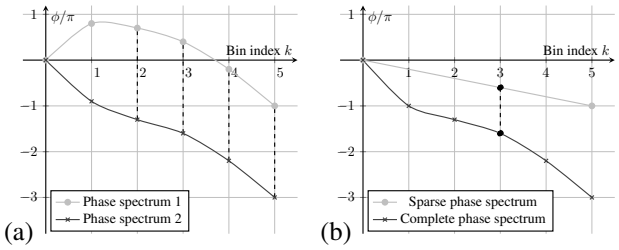

Figure 1. (a): Phase spectrum 1 and phase spectrum 2 differ only at bin index $k = 1$. Unwrapping causes an offset of 2π for all $k > 1$. (b): The light gray curve represents the data from the dark gray curve sampled at bins $k = (0, 5)$. Interpolating the sparse phase spectrum can result in an offset of π to the original data (for example at $k = 3$). The result is of limited use also for any other offsets that arise.

Summing up, the usefulness of phase interpolation is questionable under the given circumstances. Phase interpolation along the angle seems to cause less problems than interpolation along frequency but more insight is required.

Note that some directivity data sets provide phase data in frequency bands. Presumably, the data have been obtained by averaging the original phase spectrum as performed in [4]. The usefulness of averaged phase is entire unclear.

3. OUTLINE OF THE THEORY

The term *directivity* with regard to acoustic sources has been defined in various ways in the literature [5, 18, 19], [20, p. 204]. Here, we define directivity as the spatio-temporal transfer function (STTF) of a sound source under free-field conditions, evaluated at arbitrary spatial locations. This is the most general definition, from which the others above can be derived. We will assume that the directivity is evaluated on a spherical surface centered around the source.

A source directivity $W(r, \boldsymbol{\gamma}, \omega)$ is dependent on an angular frequency ω, in rad./sec, a radial distance r in m from the nominal source center, and an angle 3-vector $\boldsymbol{\gamma}$ defined interns of azimuth angle α and colatitude β. It is defined as

$$W(r, \boldsymbol{\gamma}, \omega) = \sum_{l=0}^{\infty} \sum_{m=-l}^{l} \underbrace{\breve{W}_{l,m}(\omega) h_l^{(1)}\left(\frac{\omega r}{c}\right)}_{=\mathring{W}_{l,m}(r,\omega)} Y_{l,m}(\boldsymbol{\gamma})\,, \quad (2)$$

and represents the radiated acoustic field exterior to a sphere that is just large enough to completely enclose the sound source [20, p. 206]. $h_l^{(1)}(\cdot)$ is the lth order spherical Hankel function of first kind, and $Y_{l,m}(\boldsymbol{\gamma})$, defined for integer $l \geq 0$ and $-l \leq m \leq l$, are the SH basis functions, which we are assuming to be purely real. $\breve{W}_{l,m}(\omega)$ are coefficients that contain all information about the source directivity.

The coefficients $\breve{W}_{l,m}(\omega)$ follow from an approximation to

$$\breve{W}_{l,m}(\omega) = \frac{1}{h_l^{(1)}\left(\frac{\omega R}{c}\right)} \iint_{S^2} W(R, \boldsymbol{\gamma}, \omega) Y_{l,m}(\boldsymbol{\gamma}) d\Omega \,, \tag{3}$$

where $W(R, \gamma, \omega)$ is a directivity known on a spherical surface with radius R that encloses the source, and S^2 represents the unit sphere. Alternatively, a least-squares fit of the coefficients to the spatially discrete measurement data points can be performed based on (2) [1, 21, 22]. In either case, only the coefficients up to a given order $l = L$ that depends on the number and distribution of measurement points can be obtained.

Evaluating the directivity $W(r, \gamma, \omega)$ in the limit of $r \to \infty$ [20, p. 204], leads to the large-argument approximation of the spherical Hankel function, and (2) simplifies to [20, p. 204]

$$W_\infty(r, \boldsymbol{\gamma}, \omega) = \frac{\mathrm{e}^{\mathrm{i}\frac{\omega r}{c}}}{r} \frac{c}{\mathrm{i}\omega} \sum_{l=0}^{\infty} \sum_{m=-l}^{l} (-\mathrm{i})^l \breve{W}_{l,m}(\omega) Y_{l,m}(\boldsymbol{\gamma}) \,. \tag{4}$$

$W_\infty(r, \boldsymbol{\gamma}, \omega)$ is referred to as the *far-field signature* of the directivity [23, p. 81]. Eq. (4) tells us that at sufficient distance, a source of finite spatial extent radiates spherical wave fronts ($e^{\mathrm{i}\frac{\omega r}{c}}/r$), the complex amplitude of which depends on the angle and is represented by the coefficients $\breve{W}_{l,m}(\omega)$. In other words, the angular dependence of the directivity is imposed onto a spherical wave. How far this sufficient distance has to be depends on the spatial extent of the source and its distance from the coordinate origin (which coincides with the nominal location of the source) and on the frequency. The observation distance has to be much larger than the largest dimension of the source. Classical polar diagrams display the magnitude of the far-field signature $W_\infty(r, \boldsymbol{\gamma}, \omega)$.

Since any relevant directivity will approximate a spherical wave in a certain range of observation distances, it was proposed in [2, 12, 24] to use the spherical wave model for the entire range of the directivity from the nominal source location to infinity. We obtain the spherical harmonic expansion coefficients by forcing the magnitude of the proposed spherical-wave-based directivity to be equal to the magnitude of the measured directivity on the measurement sphere. We will use the term *proposed* directivity representation (as opposed to the *conventional* directivity representation, Eq. (2)) in the remainder of this paper to refer to this representation. We refer the reader to [12, 25] for details on the concept.

It is unclear at this point how to model the phase of the directivity in the proposed approach. As discussed in Sec. 2, in most cases, there is no useful phase information available. A safe approach is to fit a minimum phase or linear phase [17] function to the modeled magnitude directivity to impose the time-domain structure of the signals. Other options are conceivable. Also, augmentation of the data through recovery of the algebraic sign of lobes in the directivity as proposed in [26] may be applied.

4. EXAMPLE 1: COMMON LOUDSPEAKER FORMAT

The Common Loudspeaker Format (CLF) [5] was proposed to allow for incorporating loudspeaker directivities in room acoustic simulations. v1 supports magnitude data on octave bands, and v2 in 3rd-octave bands. Phase information cannot be included currently. A large number of loudspeaker models are available on the website [5]. These data sets typically exhibit sufficiently dense angular sampling, but the restriction of frequency bands makes the data sparse with respect to frequency sampling.

We produced a CLF-like data from the extensive measurement data on the IEM Loudspeaker Cube, a compact loudspeaker with a cube-shaped enclosure, provided in [27, 28]. This allows us to verify the resulting directivity against the ground truth. The directivity was available as impulse responses measured on 648 equi-angularly spaced points with a spacing of 10° on a spherical surface of radius 0.75 m. The propagation delay from the loudspeakers to the measurement surface is not contained in the impulse responses. A sufficient amount of silence was therefore pre-padded before the processing to maintain causality of the ground truth data. The IEM Loudspeaker Cube comprises four identical drivers. We used the data of driver 1 in the following. We averaged the measured magnitude transfer function on a linear scale in third octave bands. Fig. 2 depicts the original magnitude transfer functions as well as the averages, which essentially constitute a data set in CLF.

We proceeded as follows to produce a complete spherical harmonic representation from the CLF-like data:

- We linearly interpolated the magnitude data on a linear scale over frequency for each direction for which data were available and performed an optional third-octave smoothing (cf. Fig. 2, black curve). It is unclear at this stage if the third octave smoothing is beneficial at all. We applied it for ease of visibility. The interpolated spectrum matches the CLF data points perfectly if no smoothing is applied. Other interpolation methods are conceivable. Note that it is unclear at this stage whether interpolation of magnitudes is favorable on a linear scale or on logarithmic one. Contradictory results have been presented [14, 15].
- We fitted a minimum-phase spectrum to the obtained magnitude spectra.
- We added a delay corresponding to the travel time from the coordinate origin to the measurement surface to maintain causality.
- We performed an unregularized least-squares fit of 6th-order SH coefficients on the complex spectra. The result is depicted in Fig. 2.

Note that a set of SH coefficients of a given order cannot perfectly represent arbitrary measurement data because the measurement data may be of a higher order. The frequency-dependency and the angular dependency of the

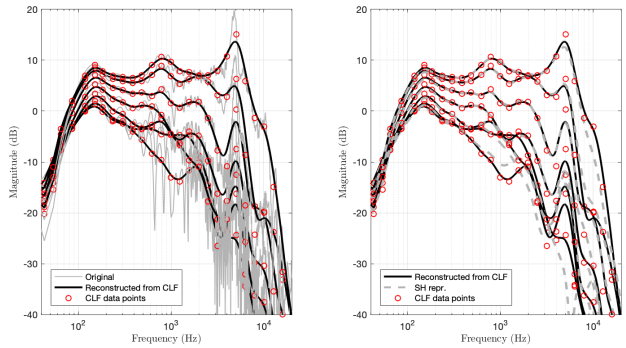

Figure 2. Selected transfer functions of the loudspeaker in the horizontal plane (gray), averaged in third octaves (red), reconstructed from the third-octave averages (black solid), computed from the proposed SH representation (gray dashed)

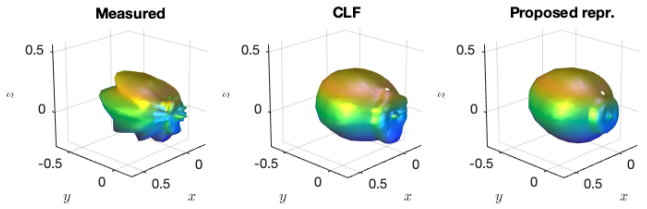

Figure 3. Balloon plots of the loudspeaker's directivity at 1 kHz. Original data (left), 3rd-octave smoothed CLF-like data (middle), and proposed SH representation (right). The distance of a point on the hull from the coordinate origin represents the magnitude of the directivity in the given direction on a linear scale.

directivity are not independent in an SH representation. One therefore has to expect that the data reconstructed from the SH decomposition at the measurement locations will depart somewhat from the data onto which the SH coefficients were fitted. This is evident in Fig. 2 (black curves vs. gray dashed curves in the subplot on the right). This is an inherent property of SH representations that cannot be avoided. The classical order-limited SH decomposition causes a significant roll-off of the time-frequency spectrum towards higher frequencies [29], which is not apparent with the proposed representation [12, Fig. 1]. The latter causes only moderate deviations.

Note that it can actually be an advantage in some situations that the SH fitting modified the magnitude of the time-frequency transfer function as we will demonstrate in Sec. 5. Fig. 3 shows example balloon plots of the original measurement data as well as of the SH representation. A certain amount of details is lost in the SH representation because of the required order limitation.

As an application example, Fig. 4 depicts the time evolution of the acoustic field in an FDTD simulation, using directivity data for the IEM loudspeaker cube, fitted to 6th order, using both conventional and proposed representations. A Gaussian signal is used as input. The zone corresponding to the driving distribution is indicated by a white

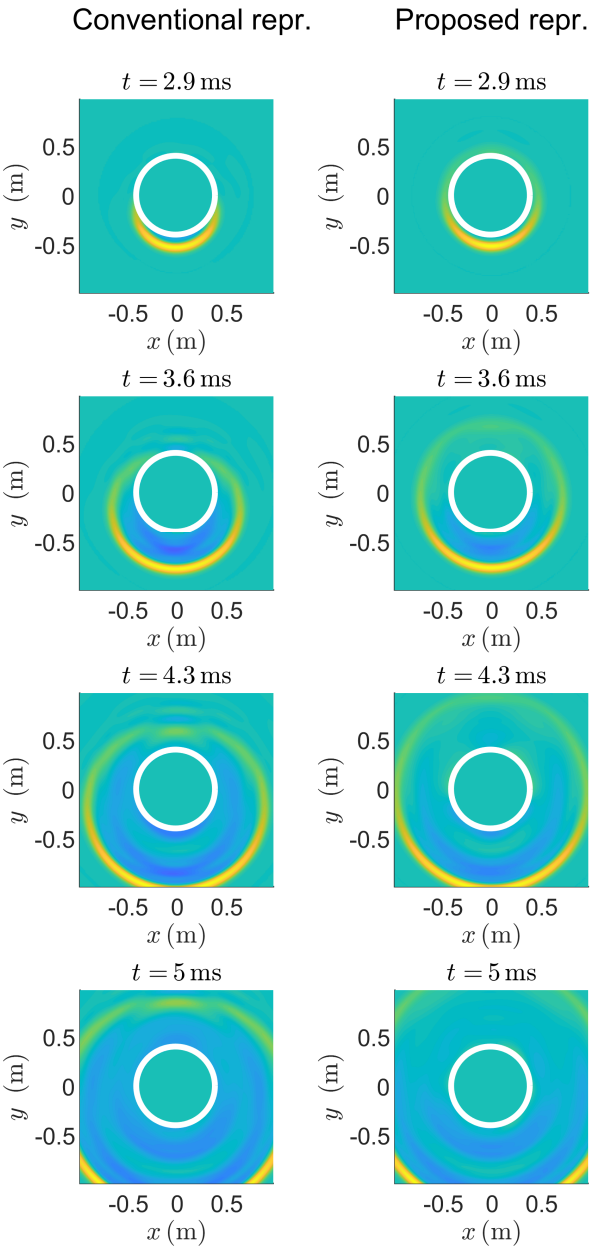

Figure 4. Time evolution of a cross-section of the simulated acoustic field emitted by the IEM Loudspeaker Cube, at times as indicated, using a Gaussian input signal of variance 1×10^{-4}. Here we use the directivity data of loudspeaker 1, with a conventional representation (left) and the proposed representation (right).

circle. We refer the reader to the Appendix for details on the FDTD simulation framework.

The spherical curvature of the wave fronts of the proposed directivity representation is evident in the right column in Fig. 4. In Fig. 5, directivity plots for the same data set are shown, at various frequencies, here using output signals drawn directly from the FDTD simulation over a sphere of radius 0.75 m. The 6th order representations, both conventional and proposed, give excellent agreement with the original measured directivity data.

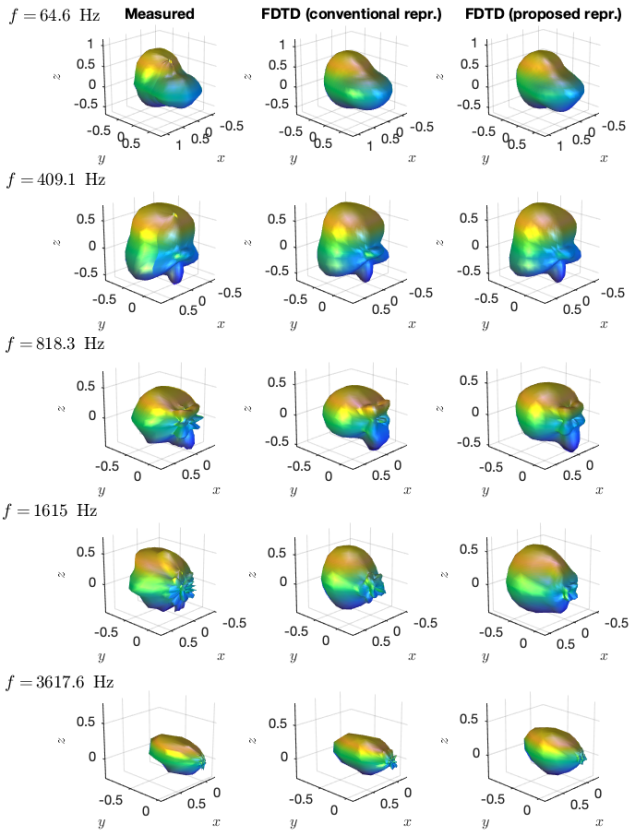

Figure 5. Normalized directivity for FDTD output of the data from Fig. 4 taken over a sphere of radius 0.75 m, and at frequencies as indicated. Left: measured directivity. Middle: 6th order conventional representation. Right: 6th order proposed representation.

5. EXAMPLE 2: SINGING VOICE

The database [30] that accompanies [7] contains recordings of two classical singers performing a glissando over one octave (i.e., a complex tone sweep). The set of partials may be interpreted as a staggered sweep over a wide frequency range so that the corresponding impulse responses that represent the directivity of the voice can be computed via deconvolution. The recordings were made with two circular microphone arrays with 32 elements each and placed along the horizontal and median planes, respectively, at a distance of 1 m from the singer's head. Effectively, only 62 measurement points are available due to coincidence of two of the microphones. We used the data from the file `IR_a_long_sweep.mat`. Fig. 6 illustrates the measurement locations.

Contrary to the CLF example from Sec. 4, which was sparse with respect to the sampling of the frequency axis, the deconvolution produces data points at all possible frequency bins. We can still not perform a classical SH decomposition like in (3) or a classical fit of SH coefficients because the data set is sparse with respect to the angular sampling. It is not possible to obtain a general directivity representation as in (2) from these data for higher than 1st order although the measurement points allow for

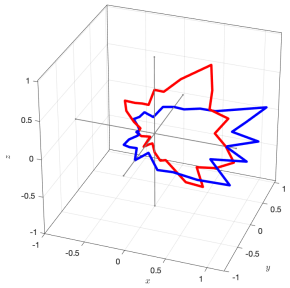

Figure 6. Reduced balloon plot for the measured directivity of the singing voice at $f = 2.0$ kHz. The horizontal and vertical data points are connected by straight lines and are plotted in different colors.

a 15th-order decomposition in each of the two measurement planes [31, Eq. (4.26)]. The approach for covering solid angle ranges at which no data are available that was presented in [22] is not able to mitigate this. Spatial upsampling [32, 33] may be able to do so, whereby the user has to guess a parametric model that approximates the observed directivity. This is feasible for a singing voice but more challenging for other types of sound sources and has not been tested for such low orders of the initial data.

Based on our approach from Sec. 3, we applied the following procedure to obtain a high-order SH directivity representation based on the available data:

- The measured transfer functions are very noisy. We therefore applied third-octave-band smoothing to the measured transfer functions (cf. Fig. 7).
- We manually set the magnitude directivity to a constant value at very low and very high frequencies where no reliable measurement data are available.
- We applied rotation about the x-axis to spatially linearly interpolate the magnitude on a logarithmic scale between the horizontal and vertical measurement locations for each frequency bin as illustrated in Fig. 8. The positions of the interpolated measurement points are obtained via the standard rotation matrix in Cartesian coordinates. The interpolation of the magnitude is performed as

$$D(\omega) = \frac{\theta}{\pi/2} D_h(\omega) + \frac{\pi/2 - \theta}{\pi/2} D_v(\omega)\,, \qquad (5)$$

  whereby θ is the angle in radians by which the horizontal points are rotated towards the vertical ones, and $D_h(\mathbf{r}_i, \omega)$ and $D_v(\mathbf{r}_i, \omega)$ are the magnitudes of the horizontal and vertical measured data points between which the interpolation is performed. This procedure is performed for all octants separately.
- We fitted a minimum phase to all magnitude data.
- We added a delay corresponding to the travel time from the coordinate origin to the measurement surface to maintain causality.

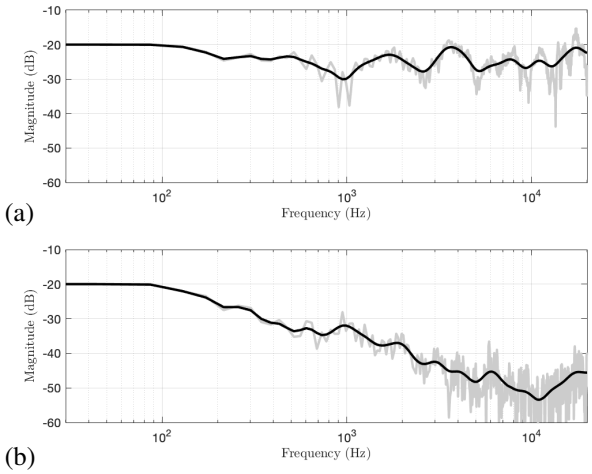

Figure 7. Transfer functions of the singing voice (gray) as well as the 3rd-octave smoothed transfer functions (black) for two selected directions

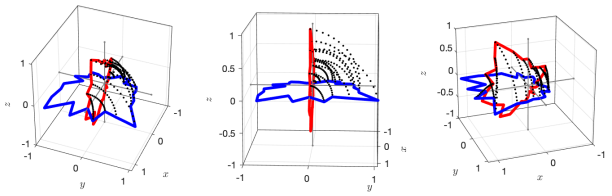

Figure 8. Balloon-plot-like snapshot of the interpolation procedure from three different angles. The black dots mark the data points obtained through interpolation.

- We performed an unregularized least-squares fit of SH coefficients on the complex spectra. We arbitrarily chose order 9 for this.
- We finally reference the directivity to the direction straight ahead as any voice signal that we might want to feed the directivity with needs to be recorded from a given direction so that the recorded signal has the source directivity for that direction embedded. It is unclear at this state if such detailed referencing is ideal given the noisiness of the measurement data. A more gentle referencing is conceivable.

Fig. 9(a) depicts the resulting directivity for one selected frequency. Fig. 10 depicts the corresponding transfer functions for different directions inside the horizontal plane. It is evident from Fig. 10 that the resulting magnitude transfer functions are more erratic than one would intuitively expect. The most plausible reason is the circumstance that the measurement data are very noisy (recall Fig. 7). The wigglyness apparent in Fig. 10 can either be reduced by applying more aggressive smoothing of the original data before the SH decomposition. Alternatively, the SH fit can be modified according to [34, Eq. (9)], where a Tikhonov regularization is proposed that penalizes higher SH orders more than lower ones. The energy in the higher

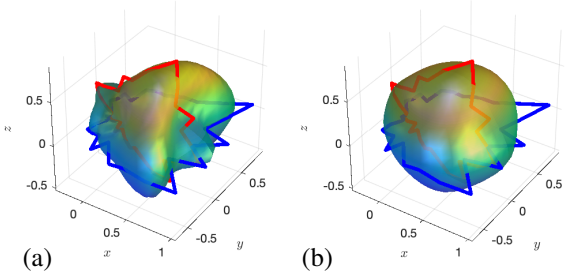

Figure 9. Balloon plot of the resulting 9th-order proposed SH representation of the singing voice at at $f = 2.0$ kHz. The original measured data points are also indicated. Unregularized SH coefficient fit (a) and regularized coefficient fit (b).

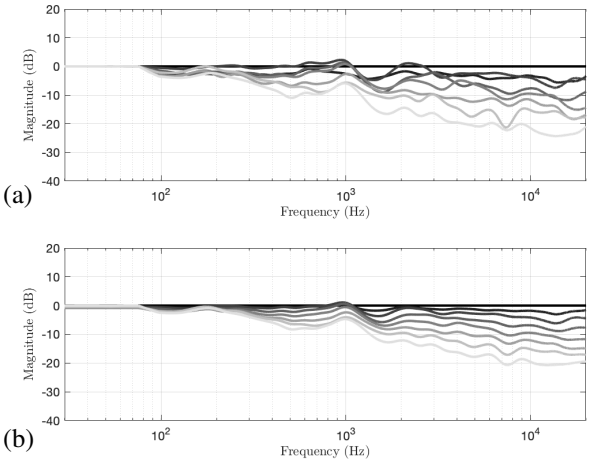

Figure 10. Transfer functions of the singing voice's directivity in the horizontal plane in steps of 24° computed directly from the SH representation. Black color represents the direction straight ahead; brighter color represents directions further towards the rear; the brightest curve represents the azimuth 168°. (a): unregularized SH coefficient fit. (b): regularized coefficient fit.

orders is thereby reduced. This produces smoother results than without regularization as evident from Fig. 10(b). A consequence is, of course, that also the angular dependency of the directivity changes, cf. Fig. 9(b). It is unclear at this stage in what situations what amount of regularization is favorable. Comparing Fig. 9(a) and (b) with polar diagrams created based on other voice directivity data such as [3, 33] suggests that Fig. 9(b) coincides better with previously published results.

6. CONCLUSIONS

We presented application examples for a previously published approach for creating spherical harmonic (SH) representations of sound source directivities. The approach imposes an angular-dependent directivity onto a spherical wave and thereby mimicks the far-field approximation of the original directivity. The examples we presented demonstrate that the approach allows for creating com-

plete SH representations even from very sparsely available data. Note that even one single data point is enough. This allows for incorporating any available directivity data set into even advanced applications. Our results based on a loudspeaker directivity show that the proposed directivity representation deviates only marginally from the conventional representation if the sound source is compact.

The presented directivity representations are publicly available [35].

APPENDIX: OUTLINE OF THE FDTD SIMULATION FRAMEWORK

Volumetric time-domain acoustic simulation methods (such as the finite difference time domain method, or FDTD) have seen increasing use since their first appearance in the early 1990s [36, 37]. Source directivity in FDTD has been approached by various authors [2, 38–40], and most recently in [1], which describes a procedure for inserting spherical harmonic encoded source directivity into an FDTD simulation.

As an example, we showed in [1] that a directivity that is available as a set of SH coefficients $\mathring{W}_{l,m}(R,\omega)$ (cf. (2)) over a sphere of finite radius R centered around the source can be directly substituted into an FDTD simulation, with appropriately defined SH driving terms. The input signals $\hat{a}_{l,m}(\omega)$ to the FDTD simulation can be computed via

$$\hat{a}_{l,m}(\omega) = \frac{4\pi c\,(-1)^l\,\mathrm{i}^l}{(\mathrm{i}\omega)^{l+1} h_l^{(1)}\left(\frac{\omega R}{c}\right)}\,\mathring{W}_{l,m}(R,\omega)\,. \qquad (6)$$

Note that the time-domain representation of the signals $\hat{a}_{l,m}(\omega)$ in (6) is injected into the FDTD simulation, which requires the directivity to be available at any possible frequency bin in the frequency range of interest or as impulse responses.

Eq. (6) may be used with both conventional and proposed directivity representations as we demonstrate in Fig. 4 and 5. All simulations are run at 44.1 kHz, using a basic 7-pt scheme, and using second order Engquist-Majda absorbing boundary conditions [41] over a cubic domain of side length 2 m.

7. REFERENCES

[1] S. Bilbao, J. Ahrens, and B. Hamilton, "Incorporating source directivity in wave-based virtual acoustics: Time-domain models and fitting to measured data," *J. Acoust. Soc. Am.*, vol. 146, no. 4, pp. 2692–2703, 2019.

[2] R. Mehra, L. Antani, S. Kim, and D. Manocha, "Source and listener directivity for interactive wave-based sound propagation," *IEEE Trans. Visualization Comp. Graphics*, vol. 20, no. 4, pp. 83–94, 2014.

[3] D. Cabrera, P. J. Davis, and A. Connolly, "Long-term horizontal vocal directivity of opera singers: Effects of singing projection and acoustic Environment," *Journal of Voice*, vol. 25, no. 6, pp. e291–e303, 2011.

[4] N. Shabtai, G. Behler, M. Vorländer, and S. Weinzierl, "Generation and analysis of an acoustic radiation pattern database for forty-one musical instruments," *J. Acoust. Soc. Am.*, vol. 141, no. 2, pp. 1246–1256, 2017. Data available online at `http://dx.doi.org/10.14279/depositonce-5861.2` (Last viewed 23/09/2019).

[5] CLF Group, "Common loudspeaker format." Available online at `http://www.clfgroup.org/` (Last viewed 06/05/2019), 2019.

[6] J. G. Tylka, R. Sridhar, and E. Y. Choueiri, "A database of loudspeaker polar radiation measurements," in *139th Convention of the AES, e-Brief 230*, (New York, NY, USA), Oct./Nov. 2015.

[7] M. Brandner, M. Frank, and D. Rudrich, "DirPat—Database and Viewer of 2D/3D Directivity Patterns of Sound Sources and Receivers," in *144th Convention of the AES*, (Milan, Italy), p. eBrief:425, May 2018.

[8] P. Mioduszewski and J. A. Ejsmont, "Directivity of tire/road noise emission for selected tires and pavements," *Noise Control Engineering Journal*, vol. 57, no. 2, pp. 129–138, 2009.

[9] D. Thompson, *Railway Noise and Vibration*. New York: Elsevier Science, 2010.

[10] S. Oerlemans and J. G. Schepers, "Prediction of wind turbine noise and validation against experiment," *Aeroacoustics*, vol. 8, no. 6, pp. 555–584, 2009.

[11] D. Griffin and J. Lim, "Signal reconstruction from short-time Fourier transform magnitude," *IEEE Trans. Acoustics, Speech, and Sig. Proc.*, vol. 31, no. 4, pp. 986–998, 1983.

[12] J. Ahrens and S. Bilbao, "Interpolation and range extrapolation of sound source directivity based on a spherical wave propagation model," in *IEEE ICASSP*, (Barcelona, Spain), May 2020.

[13] J. Zaar, "Phase unwrapping for spherical interpolation of head-related transfer functions." Diplom Thesis, University for Music and Dramatic Arts, Graz, 2011.

[14] F. Brinkmann and S. Weinierl, "Comparison of head-related transfer functions pre-processing techniques for spherical harmonics decomposition," in *AES Int. Conf. on Audio for Virtual and Aug. Reality*, (Redmond, WA, USA), Aug. 2018.

[15] G. D. Romigh, D. S. Brungart, R. M. Stern, and B. D. Simpson, "Efficient real spherical harmonics representation of head-related transfer functions," *IEEE Journal of Selected Topics in Signal Proc.*, vol. 9, no. 5, pp. 921–930, 2015.

[16] C. Andersson, "Headphone auralization of acoustic spaces recorded with spherical microphone arrays." Master's thesis, Chalmers University of Technology, 2017.

[17] B. Girod, R. Rabenstein, and A. Stenger, *Signals and Systems*. New York: J.Wiley & Sons, 2001.

[18] J. Meyer, *Acoustics and the Performance of Music*. New York: Springer, 2009.

[19] D. Blackstock, *Fundamentals of Physical Acoustics*. New York, NY: Wiley-Interscience, 2000.

[20] E. Williams, *Fourier Acoustics: Sound Radiation and Nearfield Acoustical Holography*. New York: Academic Press, 1999.

[21] D. N. Zotkin, R. Duraiswami, and N. Gumerov, "Regularized HRTF fitting using spherical harmonics," in *IEEE WASPAA*, (New Paltz, NY, USA), pp. 257–260, Oct. 2009.

[22] J. Ahrens, M. R. P. Thomas, and I. Tashev, "HRTF magnitude modeling using a non-regularized least-squares fit of spherical harmonics coefficients on incomplete data," in *Proc. of APSIPA*, (Hollywood, CA, USA), pp. 1–5, December 2012.

[23] N. Gumerov and R. Duraiswami, *Fast Multipole Methods for the Helmholtz Equation in Three Dimensions*. Amsterdam: Elsevier, 2005.

[24] J. Ahrens and S. Spors, "Wave field synthesis of moving virtual sound sources with complex radiation properties," *J. Acoust. Soc. Am.*, vol. 130, no. 5, pp. 2807–2816, 2011.

[25] J. Ahrens and S. Bilbao, "Computation of spherical harmonic representations of source directivity based on the finite-distance signature," *IEEE Trans. TASPL*, 2020. (accepted).

[26] F. Zagala and F. Zotter, "Idea for sign-change retrieval in magnitude directivity patterns," in *Proc. of DAGA*, (Rostock, Germany), pp. 1–4, 2019.

[27] N. Meyer-Kahlen, F. Zotter, and K. Pollack, "Design and measurement of first-order, horizontally beam-controlling loudspeaker cube," in *144th Convention of the AES, e-Brief 447*, (Milan, Italy), May 2018.

[28] F. Zotter, "High-resolution directional impulse responses of the iem loudspeaker cubes." Available online at `https://phaidra.kug.ac.at/detail_object/o:70240` (Last viewed 06/05/2019), 2019.

[29] N. Hahn and S. Spors, "Physical properties of modal beamforming in the context of data-based sound reproduction," in *139th Convention of the AES*, (New York, NY, USA), p. 9468, Oct. 2015.

[30] M. Brandner, "DirPat Repository Element: Directivity Measurements of a Classical Singer." Available online at `https://phaidra.kug.ac.at/detail_object/o:76751` (Last viewed 09/23/2019), 2018.

[31] J. Ahrens, *Analytic Methods of Sound Field Synthesis*. Heidelberg, Germany: Springer, 2012.

[32] C. Pörschmann, J. M. Arend, and F. Brinkmann, "Directional equalization of sparse head-related transfer function sets for spatial upsampling," *IEEE/ACM TASLP*, vol. 27, no. 6, pp. 1060–1071, 2019.

[33] C. Pörschmann and J. M. Arend, "A method for spatial upsampling of directivity patterns of human speakers by directional equalization," in *Proc. of DAGA*, (Rostock, Germany), 2019.

[34] R. Duraiswami, D. Zotkin, and N. Gumerov, "Interpolation and range extrapolation of HRTFs," in *IEEE ICASSP*, (New Paltz, NY, USA), pp. 257–260, Oct. 2004.

[35] J. Ahrens, "Database of spherical harmonic representations of sound source directivities." Zenodo, DOI: 10.5281/zenodo.3707708, available online also at `https://github.com/AppliedAcousticsChalmers/sound-source-directivities/`, 2020.

[36] D. Botteldooren, "Acoustical finite-difference time-domain simulation in a quasi-cartesian grid," *J. Acoust. Soc. Am.*, vol. 95, no. 5, pp. 2313–2319, 1994.

[37] L. Savioja, T. Rinne, and T. Takala, "Simulation of room acoustics with a 3-D finite-difference mesh," in *Proc. Int. Compu. Music Conf.*, (Århus, Denmark), pp. 463–466, sep 1994.

[38] J. Escolano, J. Lopez, and B. Pueo, "Directive sources in acoustic discrete-time domain simulations based on directivity diagrams," *JASA Express Lett.*, vol. 121, pp. 256–262, 2007.

[39] A. Southern and D. Murphy, "Low complexity directional sound sources for finite difference time domain room acoustic models," in *Proc. 126th Audio Eng. Soc. Conv.*, (Munich, Germany), 2009.

[40] S. Bilbao and B. Hamilton, "Directional sources in wave-based acoustic simulation," *IEEE Trans. Audio Speech Language Proces.*, vol. 27, pp. 415–428, 2019.

[41] B. Engquist and A. Majda, "Absorbing boundary conditions for the numerical evaluation of waves," *Math. Comp.*, vol. 31, no. 139, pp. 629–651, 1997.